nature photonics

ARTICLES

https://doi.org/10.1038/s41566-019-0380-z

Optically controlling the emission chirality of microlasers

N. Carlon Zambon[1,4*], P. St-Jean[1,4*], M. Milićević[1], A. Lemaître[1], A. Harouri[1], L. Le Gratiet[1], O. Bleu[2], D. D. Solnyshkov[2], G. Malpuech[2], I. Sagnes[1], S. Ravets[1], A. Amo[3] and J. Bloch[1]

Orbital angular momentum (OAM) carried by helical light beams is an unbounded degree of freedom that offers a promising platform in modern photonics. So far, integrated sources of coherent light carrying OAM are based on resonators whose design imposes a single, non-tailorable chirality of the wavefront (that is, clockwise or counterclockwise vortices). Here we propose and demonstrate the realization of an integrated microlaser where the chirality of the wavefront can be optically controlled. Importantly, the scheme that we use, based on the optical breaking of time-reversal symmetry in a semiconductor microcavity, can be extended to different laser architectures, thus paving the way to the realization of a new generation of OAM microlasers with tunable chirality.

Harnessing the physical properties of light, for example, its frequency, amplitude, wavevector and angular momentum, is ubiquitous in photonic technologies. Among these various degrees of freedom, angular momentum emerging from the spin moment of photons (related to their circular polarization) has been proven to be extremely powerful because it can be easily controlled with linear optical elements such as waveplates and polarizers.

Since the pioneering work of Allen and colleagues[1], it is now well known that light's angular momentum is not restricted to the spin moment of photons. It can also emerge, in the paraxial regime, by structuring helical phase fronts $e^{i\ell\phi}$, where the quantum number ℓ describes the number of times the phase of the wavefront winds around the direction of propagation within an optical period. The most notable asset of this degree of freedom, usually referred to as the orbital angular momentum (OAM), is that, contrary to its spin counterpart which is restricted to values of $\pm\hbar$, it is theoretically unbounded; for example, generation of light vortices carrying more than 10^4 quanta of OAM has recently been demonstrated[2].

Over the past decade, numerous proposals and demonstrations that take advantage of this unbounded Hilbert space have emerged. For instance, it has been acknowledged that these higher-dimensional quantum states could offer a drastically enhanced information density, both in classical[3–6] and quantum[7–9] communication channels, and they could also allow improvements to the resilience against noise and eavesdropping of quantum communication protocols[10,11]. Moreover, the ability to transfer large quanta of OAM to massive objects has led to the development of novel techniques in optical manipulation[12–14] and in optomechanics[15]. From a fundamental point of view, generating and entangling quantum states with such arbitrarily large quantum numbers has been demonstrated to be a very promising avenue for investigating the foundations of quantum mechanics[2,16,17].

The growing interest in this degree of freedom of light calls for the development of coherent sources carrying well-defined and tunable OAM. One possible strategy that has been extensively explored is to shape the phase front of paraxial beams with bulk devices such as spatial light modulators[4,5]. Although these approaches have the advantage of being extremely versatile, allowing the generation of high-order vortices, they typically suffer from low operation frequencies and remain extremely difficult to integrate on a chip. Furthermore, strategies based on converting circular polarization to OAM using nanostructured metasurfaces[18–20] or q-plates[21,22] allow switching between two values of OAM. However, their full integration is also very challenging, as they rely on complex architectures involving many optical elements that are sensitive to unavoidable birefringent effects in photonic circuits.

Recent demonstrations of integrated OAM lasers based on ring resonators[23–25] are very promising. However, it is very challenging in these integrated devices to break the mirror symmetry between clockwise (CW) and counter-clockwise (CCW) propagating modes, which is necessary to generate an emission carrying a net OAM. So far, this difficulty has been succesfully overcome by engineering chiral resonators, for example by tuning the gain and loss around the resonator, but the scalability of this approach is strongly limited because the engineering of the devices imposes a given, non-tailorable chirality to the lasing mode: each device can generate only either a CW or a CCW vortex.

In this Article, we propose and demonstrate a novel scheme to achieve OAM lasing in a fully integrated device where the chirality of the emission (that is CW or CCW vortices) can be optically controlled. Although the magnitude of the OAM ($|\ell|$) is not tunable in a single device, we show that this parameter can be accurately controlled during the fabrication process by tailoring appropriately the geometry of each microlaser. Rather than relying on the engineering of a chiral resonator, our scheme is based on optically breaking time-reversal symmetry by spin-polarizing a gain medium with a circularly polarized optical pump. By taking advantage of the spin–orbit coupling of photons confined in planar microcavities with rotational symmetry[26–28], this allows us to generate a lasing emission that carries OAM with a chirality that can be controlled solely by tuning the polarization of the pump.

Spin–orbit coupling in benzene-like photonic molecules

To implement this scheme we consider a vertical cavity surface emitting laser (VCSEL) formed from a semiconductor planar

[1]Centre de Nanosciences et de Nanotechnologies (C2N), CNRS - Université Paris-Sud - Université Paris-Saclay, Palaiseau, France. [2]Institut Pascal, PHOTON-N2, Université Clermont Auvergne, CNRS, SIGMA Clermont, Clermont-Ferrand, France. [3]Univ. Lille, CNRS, UMR 8523 – PhLAM – Physique des Lasers Atomes et Molécules, Lille, France. [4]These authors contributed equally: N. Carlon Zambon, P. St-Jean. *e-mail: nicola.carlon-zambon@c2n.upsaclay.fr; philippe.st-jean@c2n.upsaclay.fr

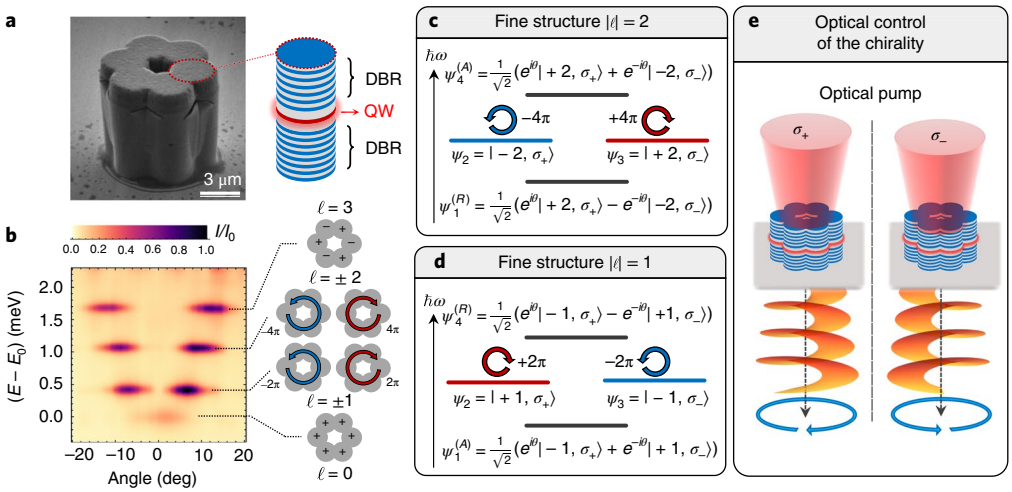

Fig. 1 | Spin–orbit coupling in benzene-like OAM lasers. a, SEM image of the benzene photonic molecule. Right, Schematic representation of a single pillar embedding a quantum well (QW) between distributed Bragg mirrors (DBR). **b**, Energy and angle-resolved photoluminescence below the lasing threshold, presenting the four OAM manifolds ($\ell = 0, \pm 1, \pm 2, 3$). The phase winding of each eigenmode (without accounting for the spin of photons) is schematically presented on the right. **c**, **d**, Fine structure of the $\ell = 2$ (**c**) and $\ell = 1$ (**d**) manifolds when the spin–orbit coupling is taken into account. Red and blue lines correspond to states carrying a net CCW and CW OAM, respectively. In modes $\psi_{1,4}$, the phase $\theta = 2\pi/6$. **e**, Schematic representation of the protocol used in this work. A circularly polarized pump ($\sigma_{\pm}$) is used to trigger lasing in a benzene photonic molecule; the lasing emission carries a net OAM whose chirality is dictated solely by the polarization of the pump.

microcavity embedding a single $In_{0.05}Ga_{0.95}As$ quantum well (details of the fabrication are presented in the Supplementary Information). In such a cavity, lasing occurs in the weak coupling regime so polariton physics is not involved above threshold. The cavity is then etched to form hexagonal rings of coupled micropillars (a scanning electron microscopy (SEM) image of a ring is presented in Fig. 1a). Owing to the hybridization of the eigenmodes of each pillar, these benzene-like photonic molecules present six eigenmodes (without considering the spin of photons) that can be classified by their angular momentum ℓ associated to the relative phase between the pillars:

$$|\ell\rangle = \frac{1}{\sqrt{6}} \sum_j e^{2\pi i \ell j/6} \, |\phi_j\rangle \qquad (1)$$

where $|\phi_j\rangle$ is the photonic ground state of the jth pillar. The four energy levels ($\ell = 0, \pm 1, \pm 2, 3$) can be observed by angle-resolved non-resonant photoluminescence measurements below the lasing threshold (Fig. 1b). As schematically depicted in the right part of Fig. 1b, the mode $\ell = 0$ presents a constant phase around the molecule and $\ell = 3$ presents a π phase shift between neighbouring pillars; therefore, these states do not exhibit a net angular momentum. In contrast, $\ell = \pm 1$ and ± 2 present phase vortices with a topological charge ℓ.

It was recently shown that, in planar microcavities with rotational symmetry[26,27], the spin moment of photons couples with their orbital angular momentum[27]. This analogous spin–orbit coupling arises from the fact that photon hopping between neighbouring pillars is polarization-dependent: the coupling is typically 5–10% greater for photons linearly polarized along the axis linking the pillars than for photons polarized perpendicularly[29]. Due to the azimuthal dependence of this anisotropic hopping, the in-plane momentum of the photons couples with their spin. Under this effect, ℓ is no longer a good quantum number and the degeneracy of the $|\ell| = 1$ and $|\ell| = 2$ manifolds is lifted, each of them presenting a three-level fine structure presented schematically in Fig. 1c,d, respectively. This fine structure cannot be probed below the lasing threshold (for example, in Fig. 1b), because the linewidths exceed the energy splittings (the ψ_{1-4} splitting is proportional to the hopping energy anisotropy, typically ~50 μeV). In the lasing regime, however, the linewidths become much smaller than the splittings, allowing the observation of emission from one single state of the manifold[27].

In this fine structure, the highest and lowest energy modes ($\psi_{1,4}$) present either a radial (R) or azimuthal (A) linear polarization, and do not exhibit orbital angular momentum. They are formed from a linear combination of CW and CCW vortices with opposite circular polarizations (see modes in Fig. 1c,d, and see Supplementary Information for their derivation). Generating a net chirality using these modes would require a precise and tunable filtering of the emission[27], an approach that is very difficult to implement on a chip. On the other hand, the degenerate middle modes present opposite circular polarizations ($\psi_{2,3}$) and carry net OAM with opposite chiralities.

To obtain lasing in a single one of these chiral modes, one needs to pump preferentially only one of these two degenerate states; here, we show that this can be achieved by spin-polarizing the active medium. Indeed, for a fully polarized medium the gain is twice as large for ψ_2 or ψ_3 (depending on the polarization) than for the radially or azimuthally polarized modes ψ_1 and ψ_4, because these latter modes exhibit a reduced overlap with the polarized reservoir stemming from the $1/\sqrt{2}$ coefficients in their wavefunction (Fig. 1c, d). Therefore, such an imbalance of the gain within each manifold allows single-mode lasing operation to be achieved in either of the chiral modes $\psi_{2,3}$ by injecting spin-polarized carriers in the device.

As presented hereafter, this spin-polarization of the gain medium can be achieved with a circularly polarized off-resonant optical pump[30,31] (as schematically presented in Fig. 1e). The chirality of the emission can thus be controlled by simply tuning the polarization of the pump. This optical breaking of time-reversal symmetry allows, in principle, ultrafast switching times limited only by the relaxation of carriers (~ps). We then show how slightly changing the geometry of the device enables control of the OAM manifold ($|\ell| = 1$ or $|\ell| = 2$) in which lasing occurs.

OAM lasing with optically controlled chirality

To demonstrate this optical control of the chirality, we investigated two different devices formed from photonic molecules with

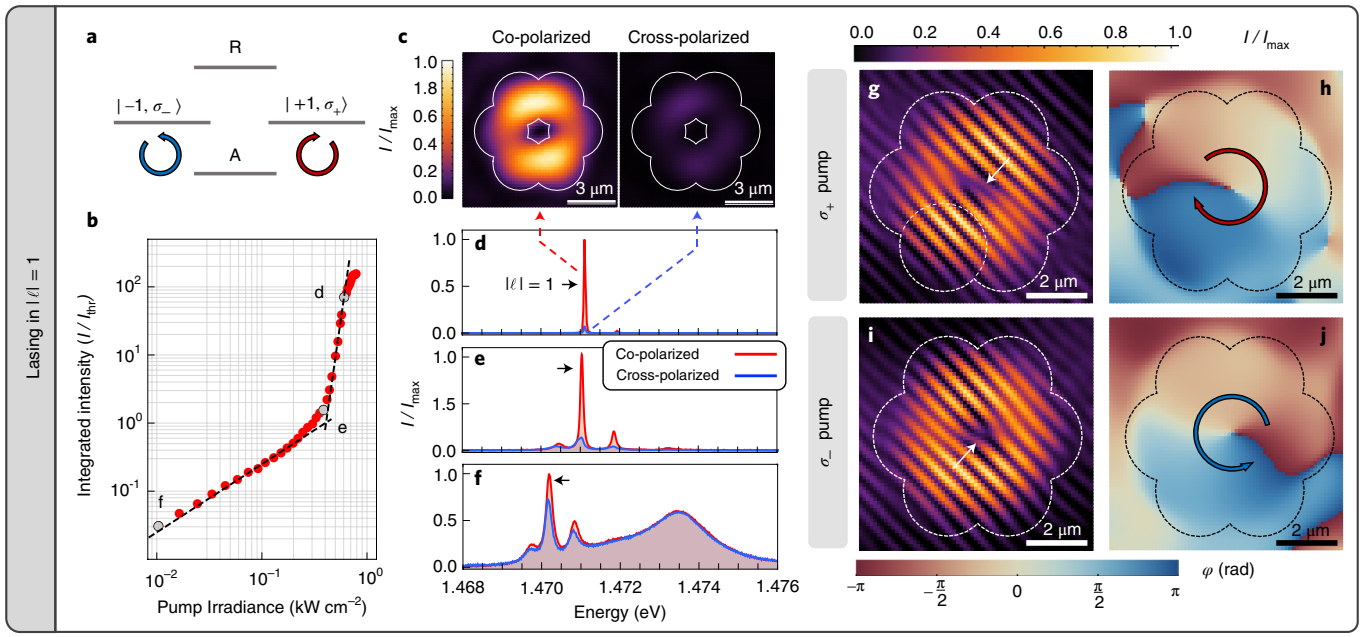

Fig. 2 | Orbital angular momentum lasing in the $|\ell| = 1$ manifold. a, Fine structure of the $|\ell| = 1$ manifold. **b**, Integrated intensity measured as a function of incident pump power showing a lasing threshold at $P_{thr} \approx 0.4\,kW\,cm^{-2}$. **c**, Co- and cross-polarized real-space images of the emission under a σ_+ polarized pump without spectral filtering. **d**–**f**, Polarization and energy resolved emission spectra under a σ_+ polarized pump above (**d**), at (**e**) and below (**f**) the lasing threshold. Red and blue curves correspond to co- (σ_+) and cross-polarized (σ_-) emission with respect to the polarization of the pump. **g**, **i**, Interference patterns measured as described in the text at $P = 0.6\,kW\,cm^{-2}$ (corresponding to **d**) for a σ_+ and σ_- polarized pump, respectively. **h**, **j**, Corresponding phase maps showing the 2π CW (CCW) vortex under a σ_+ (σ_-) pump.

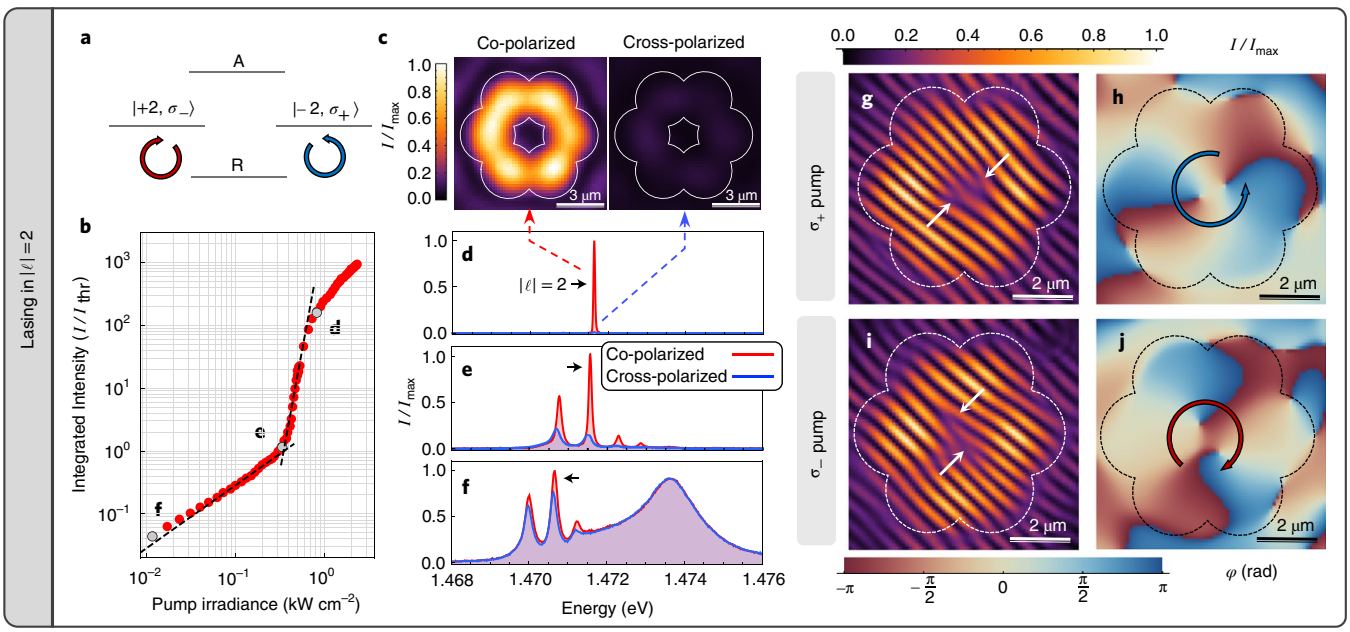

Fig. 3 | Orbital angular momentum lasing in the $|\ell| = 2$ manifold. a, Fine structure of the $|\ell| = 2$ manifold. **b**, Integrated intensity measured as a function of incident pump power showing a lasing threshold at $P_{thr} \approx 0.3\,kW\,cm^{-2}$. **c**, Co- and cross-polarized real space images of the emission under a σ_+ polarized pump. **d**–**f**, Polarization and energy resolved emission spectra under σ_+ polarized pump above (**d**), at (**e**) and below (**f**) the lasing threshold. Red and blue curves correspond to co- (σ_+) and cross-polarized (σ_-) emission with respect to the polarization of the pump. **g**, **i**, Interference patterns measured as described in the text at $P = 0.8\,kW\,cm^{-2}$ (corresponding to **d**) for a σ_+ and σ_- polarized pump, respectively. **h**, **j**, Corresponding phase maps showing 4π CCW (CW) vortex under σ_+ (σ_-) pump.

3.2-μm-diameter micropillars and an interpillar distance of 2.3 μm (molecule M1) or 2.4 μm (molecule M2). The variation of the interpillar distance modifies the relative gain/loss ratio of the photonic modes (see Supplementary Information), allowing the selection of a precise $|\ell|$ manifold in which lasing occurs: for the molecule M1 (M2), lasing occurs in the $|\ell| = 1$ ($|\ell| = 2$) manifold.

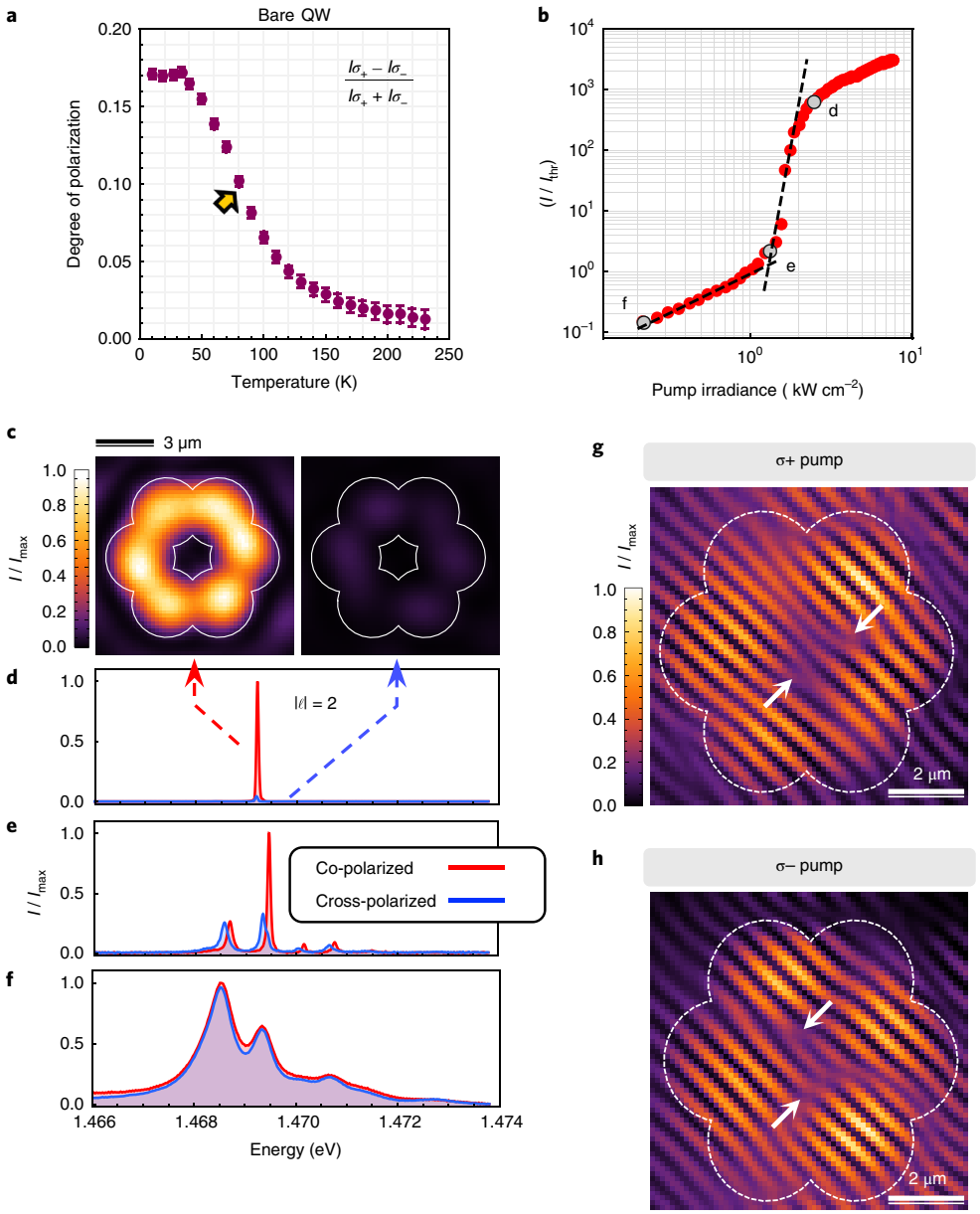

Fig. 4 | Operation at 80 K. a, Degree of circular polarization of the bare quantum well photoluminescence as a function of temperature. **b**, Integrated intensity of device M2 as a function of the pumping power. **c**, Co- and cross-polarized real-space images of the beam above the lasing threshold, under a σ_+ pump. **d**–**f**, Emission spectra, above (**d**), at (**e**) and below (**f**) the lasing regime, for a detection co- (red) and cross-polarized (blue) with respect to the σ_+ pump. **g**, **h**, Self-interference of the laser emission showing the characteristic $\pm 4\pi$ phase vortices under a σ_+ (**g**) and σ_- (**h**) pump.

The devices were held in a closed-cycle cryostat at $T = 4$ K. Figure 2 presents the results for molecule M1 when exciting the device with a circularly polarized (σ_+) off-resonant pump ($E_{\mathrm{pump}} \approx 1.6$ eV). A nonlinear increase of the integrated emission intensity is observed above a threshold power density of $P_{\mathrm{th}} = 0.4\,\mathrm{kW\,cm^{-2}}$ (Fig. 2b); emission spectra for excitation powers above, around and below this threshold are respectively presented in Fig. 2d–f. Above the threshold, we see the emergence of a single-mode emission from the $|\ell| = 1$ manifold, as well as a strong narrowing of the linewidth, being only limited by the resolution of the spectrometer (~40 μeV). This unambiguously indicates the onset of lasing in this manifold.

At low excitation power (Fig. 2f), the emission presents a non-negligible degree of polarization $\left(P = \frac{\mathcal{I}_{\sigma_+} - \mathcal{I}_{\sigma_-}}{\mathcal{I}_{\sigma_+} + \mathcal{I}_{\sigma_-}} \sim 5\%\right)$, demonstrating that spin-polarization of photogenerated carriers (imposed by conservation of angular momentum of the circularly polarized pump photons) is significantly preserved during their relaxation in the gain medium (that is, the quantum well). In the lasing regime (Fig. 2d), P is greatly enhanced, reaching almost unity ($P > 95\%$), thanks to the stimulated nature of the emission. Figure 2c presents real-space images of the device emission (without any spectral filtering) under co- and cross-polarized detection, providing evidence that the whole beam presents this strong degree of polarization. This indicates that the spin-polarized pump indeed triggers lasing in a circularly polarized mode.

To provide evidence of the phase vortex associated to this lasing mode, we interfere the beam with a magnified image of the emission from one of the molecule pillars, which acts as a phase reference. The resulting interferogram, taken without spectral or circular polarization filtering, is shown in Fig. 2g (the dashed circle indicates the reference pillar). The corresponding phase map, obtained with a standard off-diagonal Fourier filtering

technique, is presented in Fig. 2h. The pitchfork in the interferogram (marked by a white arrow) and the vortex in the phase map indicate a 2π winding of the phase around the molecule, showing that the laser mode presents an OAM of $\ell = +1$ (corresponding to $|\ell = +1, \sigma_+\rangle$ in Fig. 2a). Remarkably, when changing the excitation polarization to σ_-, the polarization of the gain medium is inverted, and the lasing mode, fully σ_- polarized, now indicates opposite chirality, corresponding to $\ell = -1$. This is evidenced by the interferogram and corresponding phase map presented in Fig. 2i,j that respectively shows an inversion of the pitchfork and of the circulation of the phase. This demonstrates the ability to optically break time-reversal symmetry and to control the chirality of the lasing mode.

Importantly, we observe a very high purity of the OAM generated, although the degree of polarization of the emission below the lasing threshold is very low (~5%). This indicates that our lasing scheme provides strongly enhanced resilience against depolarization of the excitation, in comparison to optical devices that directly convert circular polarization to OAM (for example, q-plates or metasurfaces).

When considering the second device (molecule M2), we now observe that a σ_+ polarized pump triggers lasing in the $|\ell| = 2$ manifold (see Fig. 3a for a schematic of the $|\ell| = 2$ fine structure, Fig. 3b for the *I*–*P* curve, Fig. 3c for real-space images of the beam and Fig. 3d–f for emission spectra). Similarly, as for M1, the degree of polarization of the emission in the lasing regime is very strong ($P > 95\%$) and dictated by the polarization of the pump. The phase vortex of this lasing beam is extracted using the same technique as for M1: the interferogram and corresponding phase map are presented in Fig. 3g,h, respectively. The two pitchforks in the interferogram (white arrows) and the double phase vortex clearly show that the emission now presents an OAM of $\ell = -2$. Then, by changing the polarization of the pump to σ_-, the chirality of the emission is inverted to $\ell = +2$, as shown by the interferogram and phase map presented in Fig. 3i,j.

Temperature robustness of the scheme

The possibility to control the chirality of the emission only requires that the spin-dependence of the gain within one OAM manifold dominates all other possible contributions (for example, the spectral dependence of the gain). In our case, this condition is fulfilled by optimizing the gain at the energy of a precise $|\ell|$ manifold and imprinting a sufficiently large spin-polarization in the quantum well. This latter condition can be undermined by the onset of thermally activated spin-relaxation processes. To evaluate the robustness of our devices against these processes, we measured the degree of circular polarization of the photoluminescence from a single quantum well (without the cavity) as a function of temperature, when pumped with a σ_+ polarized pump (Fig. 4a). At $T = 4$ K, the emission presents a degree of circular polarization of ~17%. Interestingly, the degree of polarization remains non-negligible (>10%) up to $T = 80$ K; at higher temperature ($T > 100$ K), it slowly vanishes below 5%.

As a result of this temperature resilience, we were able to implement our scheme up to $T = 80$ K: Fig. 4b–h shows that exciting device M2 with circular polarization still allows triggering lasing with an optically controllable OAM $\ell = \pm 2$. Above this temperature, the lasing mode approaches the GaAs bandgap[32], thus drastically enhancing the light absorption and significantly increasing the threshold power. This technical limitation prevents us from exploring the lasing regime of our structure at higher temperatures. Nevertheless, by using a pulsed excitation instead of a CW and an appropriate heterostructure design, we expect to extend the range of operation of the microlaser up to room temperature[31].

Perspectives

It is important to point out that the scheme we demonstrate here is not restricted to benzene-like molecules, but can be implemented in any *n*-pillar ring molecules with *n* even and ≥4 (see Supplementary Information for a demonstration based on symmetry group arguments). When considering *n* pillars, the $|\ell| = 1$ and $|\ell| = n/2 - 1$ manifolds present the adequate fine structure similar to that of $|\ell| = 1$ and $|\ell| = 2$ in Fig. 1c,d. This could pave the way to the implementation of microlasers generating arbitrarily large values of OAM with a tunable chirality. Using arrays of such microlasers, one could encode quantum and classical information in higher-dimension bases ($d > 2$). Moreover, the method we propose to optically break time-reversal symmetry allows, in principle, controlling the emission chirality on ultrashort timescales, limited only by the relaxation times of carriers (~ps).

Our design can be transposed to other laser architectures, because the underlying concepts (that is spin–orbit coupling of photons and spin-polarization of the gain medium) are very general. For instance, active materials with more resilient spin properties, such as transition metal dichalcogenide monolayers (for example MoS_2 and WSe_2), which present electron spin–valley locking, could enhance the robustness of the device[33]. Also, combining the present design with ferromagnetic electrodes[34] could open the possibility to fabricate OAM microlasers with electrical injection.

Finally, our results could be extended beyond the field of OAM lasers, for example in optomechanics by coherently transferring photonic angular momentum to chiral torsional modes of the microstructures[35]. Furthermore, by embedding a quantum emitter (for example, a quantum dot or semiconductor defects) in the resonator instead of a quantum well, it would be possible to generate single photons with a controllable OAM[36].

Online content

Any methods, additional references, Nature Research reporting summaries, source data, statements of data availability and associated accession codes are available at https://doi.org/10.1038/s41566-019-0380-z.

Received: 5 August 2018; Accepted: 4 February 2019;
Published online: 18 March 2019

References

1. Allen, L., Beijersbergen, M. W., Spreeuw, R. J. C. & Woerdman, J. P. Orbital angular momentum of light and the transformation of Laguerre–Gaussian laser modes. *Phys. Rev. A* **45**, 8185–8189 (1992).
2. Fickler, R., Campbell, G., Buchler, B., Lam, P. K. & Zeilinger, A. Quantum entanglement of angular momentum states with quantum numbers up to 10,010. *Proc. Natl Acad. Sci. USA* **113**, 13642–13647 (2016).
3. Gibson, G. et al. Free-space information transfer using light beams carrying orbital angular momentum. *Opt. Express* **12**, 5448–5456 (2004).
4. Wang, J. et al. Terabit free-space data transmission employing orbital angular momentum multiplexing. *Nat. Photon.* **6**, 488–496 (2012).
5. Bozinovic, N. et al. Terabit-scale orbital angular momentum mode division multiplexing in fibers. *Science* **340**, 1545–1548 (2013).
6. Willner, A. E. et al. Optical communications using orbital angular momentum beams. *Adv. Opt. Photon.* **7**, 66–106 (2015).
7. Vallone, G. et al. Free-space quantum key distribution by rotation-invariant twisted photons. *Phys. Rev. Lett.* **113**, 060503 (2014).
8. Sit, A. et al. High-dimensional intracity quantum cryptography with structured photons. *Optica* **4**, 1006–1010 (2017).
9. Erhard, M., Fickler, R., Krenn, M. & Zeilinger, A. Twisted photons: new quantum perspectives in high dimensions. *Light Sci. Appl.* **7**, 17146 (2018).
10. Kaszlikowski, D., Gnaciński, P., Żukowski, M., Miklaszewski, W. & Zeilinger, A. Violations of local realism by two entangled *N*-dimensional systems are stronger than for two qubits. *Phys. Rev. Lett.* **85**, 4418–4421 (2000).
11. Cerf, N. J., Bourennane, M., Karlsson, A. & Gisin, N. Security of quantum key distribution using *d*-level systems. *Phys. Rev. Lett.* **88**, 127902 (2002).
12. Grier, D. G. A revolution in optical manipulation. *Nature* **424**, 810–816 (2003).
13. Padgett, M. & Bowman, R. Tweezers with a twist. *Nat. Photon.* **5**, 343–348 (2011).
14. Gao, D. et al. Optical manipulation from the microscale to the nanoscale: fundamentals, advances and prospects. *Light Sci. Appl.* **6**, e17039 (2017).

15. Aspelmeyer, M., Kippenberg, T. J. & Marquardt, F. Cavity optomechanics. *Rev. Mod. Phys.* **86**, 1391–1452 (2014).
16. Collins, D., Gisin, N., Linden, N., Massar, S. & Popescu, S. Bell inequalities for arbitrarily high-dimensional systems. *Phys. Rev. Lett.* **88**, 040404 (2002).
17. Fickler, R. et al. Quantum entanglement of high angular momenta. *Science* **338**, 640–643 (2012).
18. Arbabi, A., Horie, Y., Bagheri, M. & Faraon, A. Dielectric metasurfaces for complete control of phase and polarization with subwavelength spatial resolution and high transmission. *Nat. Nanotechnol.* **10**, 937–943 (2015).
19. Devlin, R. C., Ambrosio, A., Rubin, N. A., Mueller, J. P. B. & Capasso, F. Arbitrary spin-to-orbital angular momentum conversion of light. *Science* **358**, 896–901 (2017).
20. Bouchard, F. et al. Optical spin-to-orbital angular momentum conversion in ultra-thin metasurfaces with arbitrary topological charges. *Appl. Phys. Lett.* **105**, 101905 (2014).
21. Marrucci, L., Manzo, C. & Paparo, D. Optical spin-to-orbital angular momentum conversion in inhomogeneous anisotropic media. *Phys. Rev. Lett.* **96**, 163905 (2006).
22. Naidoo, D. et al. Controlled generation of higher-order Poincaré sphere beams from a laser. *Nat. Photon.* **10**, 327–332 (2016).
23. Cai, X. et al. Integrated compact optical vortex beam emitters. *Science* **338**, 363–366 (2012).
24. Miao, P. et al. Orbital angular momentum microlaser. *Science* **353**, 464–467 (2016).
25. Peng, B. et al. Chiral modes and directional lasing at exceptional points. *Proc. Natl Acad. Sci. USA* **113**, 6845–6850 (2016).
26. Dufferwiel, S. et al. Spin textures of exciton–polaritons in a tunable microcavity with large TE-TM splitting. *Phys. Rev. Lett.* **115**, 246401 (2015).
27. Sala, V. G. et al. Spin–orbit coupling for photons and polaritons in microstructures. *Phys. Rev. X* **5**, 011034 (2015).
28. Bliokh, K. Y., Rodrguez-Fortuño, F. J., Nori, F. & Zayats, A. V. Spin–orbit interactions of light. *Nat. Photon.* **9**, 796–808 (2015).
29. Michaelis de Vasconcellos, S. et al. Spatial, spectral, and polarization properties of coupled micropillar cavities. *Appl. Phys. Lett.* **99**, 101103 (2011).
30. Ando, H., Sogawa, T. & Gotoh, H. Photon-spin controlled lasing oscillation in surface-emitting lasers. *Appl. Phys. Lett.* **73**, 566 (1998).
31. Hsu, F.-k, Xie, W., Lee, Y.-S., Lin, S.-D. & Lai, C.-W. Ultrafast spin-polarized lasing in a highly photoexcited semiconductor microcavity at room temperature. *Phys. Rev. B* **91**, 195312 (2015).
32. Sturge, M. D. Optical absorption of gallium arsenide between 0.6 and 2.75 eV. *Phys. Rev.* **127**, 768–773 (1962).
33. Wang, G. et al. Colloquium: excitons in atomically thin transition metal dichalcogenides. *Rev. Mod. Phys.* **90**, 021001 (2018).
34. Allain, A., Kang, J., Banerjee, K. & Kis, A. Electrical contacts to two-dimensional semiconductors. *Nat. Mater.* **14**, 1195–1205 (2015).
35. Fenton, E. F., Khan, A., Solano, P., Orozco, L. A. & Fatemi, F. K. Spin-optomechanical coupling between light and a nanofiber torsional mode. *Opt. Lett.* **43**, 1534–1537 (2018).
36. Fong, C. F., Ota, Y., Iwamoto, S. & Arakawa, Y. Scheme for media conversion between electronic spin and photonic orbital angular momentum based on photonic nanocavity. *Opt. Express* **26**, 21219 (2018).

Acknowledgements

The authors thank L. A. Orozco for discussions. This work was supported by ERC grant Honeypol, the H2020-FETFLAG project PhoQus (project no. 820392), the QUANTERA project Interpol (ANR-QUAN-0003-05), the French National Research Agency (ANR) projects Quantum Fluids of Light (ANR-16-CE30-0021), Labex CEMPI (ANR-11-LABX-0007), NanoSaclay (ICQOQS, grant no. ANR-10-LABX-0035), and IDEX-ISITE 16-IDEX-0001 (CAP 20-25), the French RENATECH network, the CPER Photonics for Society P4S and the Métropole Européenne de Lille via the project TFlight. P.S.-J. acknowledges financial support from the Marie Curie individual fellowship ToPol and from the Natural Sciences and Engineering Research Council of Canada. D.D.S. acknowledges the support of IUF (Institut Universitaire de France).

Author contributions

N.C.Z. and P.S.-J. performed the experiments, analysed the data and wrote the manuscript. P.S.-J. developed the group theory arguments. M.M. performed preliminary work. A.L., A.H., L.L. and I.S. grew and processed the sample. O.B., D.D.S. and G.M. provided theoretical input. S.R. participated in the experimental work and in scientific discussions. A.A. and J.B. designed the experiment and supervised the work. All authors revised the manuscript.

Competing interests

The authors declare no competing interests.

Additional information

Supplementary information is available for this paper at https://doi.org/10.1038/s41566-019-0380-z.

Reprints and permissions information is available at www.nature.com/reprints.

Correspondence and requests for materials should be addressed to N.C. or P.S.

Publisher's note: Springer Nature remains neutral with regard to jurisdictional claims in published maps and institutional affiliations.

Methods

Sample description. The benzene photonic molecules used in this work were etched out of a planar semiconductor microcavity with high quality factor ($Q \approx 4 \times 10^4$), grown by molecular beam epitaxy. The microcavity consists of a GaAs λ spacer embedded between two $Al_{0.10}Ga_{0.90}As/Al_{0.95}Ga_{0.05}As$ distributed Bragg reflectors formed from 32 (36) pairs of layers in the top (bottom) mirror. A single $In_{0.04}Ga_{0.96}As$ quantum well was inserted in the centre of the cavity to provide optical gain. The microstructure was grown on a 350-μm-thick GaAs substrate that was polished on both faces to allow operation in a transmission geometry. After the epitaxy the sample was processed with electron beam lithography and dry etching to form hexagonal arrays of coupled micropillars, with varied micropillar diameters and interpillar distances. In this work, the device investigated had a diameter of 3.2 μm and an interpillar distance of 2.3 μm (device M1) or 2.4 μm (device M2). Finally, an antireflection coating consisting of a silicon oxynitride $\lambda/4$ layer was deposited on the substrate side to avoid spurious Fabry–Pérot reflections in the substrate. A schematic of the sample is presented in the Supplementary Information.

Experimental technique. The sample was held in a closed-cycle cryostat where the temperature could be actively stabilized between 4 K and room temperature. The device was pumped on the epitaxial side with a continuous-wave Ti:sapphire laser focused by a lens with a focal length of 100 mm, producing a 20 μm FWHM Gaussian spot, ensuring a quasi-uniform illumination of the structure. The incident polarization state of the pump was controlled with a $\lambda/4$ waveplate, and its wavelength was set to 770 nm, corresponding to one of the reflectivity minima of the Bragg mirrors. The emission from the microstructure was collected in a transmission gemoetry, that is, from the substrate side, using a 0.42 NA objective. The polarization state of the emission was analysed with a polarizing beamsplitter together with a quarter-waveplate and a half-waveplate allowing the realization of a full polarization tomography. Energy resolved measurements were realized with a charge-coupled device camera coupled to a spectrometer. For measurements without spectral resolution, we used the same setup but analysed the detection at the 0th order of the spectrometer.

Data availability

The data that support the plots within this paper and other findings of this study are available from the corresponding authors upon reasonable request.